

May 17, 1999

Observability of $B_{(d)s}^0 \rightarrow \mu\mu$ decay with the CMS detector

A. Nikitenko ^{a)}

HIP, Helsinki, Finland

A. Starodumov ^{b)}

Università di Pisa e Sezione dell' INFN, Pisa, Italy

N. Stepanov ^{c)}

CERN, Geneva, Switzerland

Abstract

We have updated our previous study on the possibility to observe the rare $B_S^0 \rightarrow \mu\mu$ decay with detailed simulation of the TDR version of the CMS detector. The full simulation and reconstruction procedure has been done both for the signal and background. We improved our previous results on expected sensitivity using more sophisticated algorithms for the track and vertex reconstruction and tighter selection criteria.

^{a)} Email: Alexandre.Nikitenko@cern.ch

^{b)} Email: Andrei.Starodumov@cern.ch

^{c)} Email: Nikita.Stepanov@cern.ch

1 Introduction

The purpose of this study is to update our earlier study [1] on the possibility to observe the rare $B_S^0 \rightarrow \mu\mu$ decay with the CMS detector. As well known, this channel with a very small Standard Model branching ratio is a sensitive probe of a “new physics” affecting FCNC [2], and only the large b production rate of a hadron collider possibly allows to obtain the needed level of sensitivity. The reasons which might modify the previous results are the following (for details see the next chapters) :

- detailed simulation of the TDR version of the CMS detector, tracker in particular;
- more sophisticated algorithms for track and vertex reconstruction and tighter selection criteria;
- new version of the PYTHIA Monte-Carlo generator [3];
- improved statistical precision of the results due to a much bigger sample of generated events;
- new theoretical estimate of the branching ratio of the decay in the Standard Model $(3.5 \pm 1.0) \times 10^{-9}$

[2];

In the previous study [1] we established that the dominant background is due to direct muons from $b\bar{b}$ pairs produced through the gluon splitting mechanism. All other sources of background are found to be about one order of magnitude smaller than this one. In the present work we thus concentrated only on this source of background. The higher level trigger and kinematics selection criteria were taken as in [1]:

$$p_t^\mu > 4.3 \text{ GeV}, \quad |\eta| < 2.4 \quad (1)$$

$$0.4 < \Delta R_{\mu\mu} < 1.2, \quad p_t^{\mu\mu} > 12 \text{ GeV} \quad (2)$$

where $R_{\mu\mu}$ is the distance between the two muons in η, ϕ space and $p_t^{\mu\mu}$ is the transverse momentum of the di-muon pair. We assume that there is no significant loss of dimuon events at the first trigger level. This is justified for running at luminosity $10^{33} \text{ cm}^{-2} \text{ s}^{-1}$ but should be examined in more detail when approaching $10^{34} \text{ cm}^{-2} \text{ s}^{-1}$. To suppress the background we have exploited as in our previous study the good dimuon mass resolution of CMS, the precise two-muon vertex reconstruction, and isolation criteria with the tracker and calorimeters.

We have also investigated sensitivity to $B_d^0 \rightarrow \mu\mu$ decays.

2 Event generation

2.1 Kinematics and cross-sections

Background events have been generated by PYTHIA5.7 with default CTEQ2L structure functions and the default choice of the fragmentation function, which is the Lund symmetric fragmentation function modified for heavy endpoint quarks (see references in [3]). Pairs of $b\bar{b}$ quarks have been extracted from MSEL=1 QCD $2 \rightarrow 2$ processes where gluons are produced: process 28 (f+g \rightarrow f+g) and 68 (g+g \rightarrow g+g). Data selection kinematics cuts (1), (2) on muons have been applied at the generation level. We have generated 10000 of di-muon background events passing through these cuts.

The normalisation has been done on the $b\bar{b}$ production cross-section obtained by counting the number of events where at least one $b\bar{b}$ pair was produced. We give in Table 1 the PYTHIA output on the cross-sections of MSEL=1 subprocesses and cross-section of $b\bar{b}$ pairs production with the processes 11-13, 53 and 28,68. The total fraction of events with $b\bar{b}$ pairs is 7.4×10^{-3} and the corresponding cross-section is $409 \mu\text{b}$. According to the data in Table 1, we have normalised the background from gluon splitting on $282 \mu\text{b}$. In the previous study we normalised gluon splitting background on $370 \mu\text{b}$ given by PYTHIA5.6 with EHLQ1 structure functions (PYTHIA5.6 default).

Signal $B_S^0 \rightarrow \mu\mu$ events have been extracted from all MSEL=1 subprocesses and are present therefore a mixture of gluon splitting and gluon fusion production mechanisms.

We estimate that after trigger and kinematic selections the number of signal and background events, for one year running at luminosity $L = 10^{33} \text{ cm}^{-2} \text{ s}^{-1}$ (i.e. 10^4 pb^{-1}), is 66 and 2.9×10^7 respectively.

We checked that choosing the Peterson fragmentation function instead of the default one does not make a difference in the spectra of B-hadrons and charged particles around the B-hadron and therefore does not affect the efficiency of the kinematics selections and isolation criteria (see below). In Figure 1

are shown the spectra of the B-hadron (Figure 1a) and of charged particles (Figure 1b) with $p_t > 0.9$ GeV (not including decay products of B-hadron) in cone $\Delta R < 0.4$ around the B-hadron for the default choice of the fragmentation function (solid line) and the Peterson fragmentation function [4] (dashed line). For this plot, $b\bar{b}$ pairs have been generated by a gluon fusion mechanism $gg \rightarrow b\bar{b}$ with $\hat{p}_t > 4$ GeV. There is almost no difference between the two choices of the fragmentation function.

Table 1. Cross-sections for MSEL=1 subprocesses and corresponding cross-sections for bb pair production in these processes.

| Subprocesses | | Cross-section (mb) | Cross-section of bb pairs production (mb) |
|--------------|---------------------------|--------------------|---|
| I | 11 f + f' -> f + f' (QCD) | I 1.528E+00 | I |
| I | 12 f + f~ -> f' + f~' | I 2.209E-02 | I 0.002 |
| I | 13 f + f~ -> g + g | I 2.086E-02 | I |
| I | 53 g + g -> f + f~ | I 8.553E-01 | I 0.125 |
| I | 28 f + g -> f + g | I 1.659E+01 | I |
| I | 68 g + g -> g + g | I 3.621E+01 | I 0.282 |
| I | All included subprocesses | I 5.522E+01 | I 0.409 |

2.2 CMS detector simulation

Detector simulation has been done with the CMSIM package [5] which is based on GEANT3 and simulates properly the response of the CMS subdetectors used for the reconstruction. The TDR designs for the calorimetry and tracker are taken. Two options of the tracker geometry have been simulated, corresponding to the low and high luminosity running. The important difference between these two designs is the position of the pixel vertex detector. The radii of the two barrel pixel cylinders are 4 and 7 cm for the low luminosity design, and 7 and 11 cm for the high luminosity case. The low luminosity configuration provides a better vertex reconstruction precision over the entire tracker acceptance [6].

Both signal and background events were passed through the detailed detector simulation and reconstruction procedure to obtain the efficiency of the selection criteria. Energy thresholds on particle tracking is taken as 100 KeV (1 MeV) for electrons and photons, and 1 MeV (10 MeV) for hadrons in the Tracker (Calorimetry).

3 Event selections

3.1 Track and vertex reconstruction

The CM_FKF track finder [6] was used to reconstruct all tracks with $p_t \geq 0.9$ GeV, $|\eta| \leq 2.5$ with at least 6 hits and $\chi^2/ndf \leq 7$. In these conditions, the global track reconstruction efficiency is about 91 % both for signal and background samples. After track reconstruction the GVF vertex finder [7] was implemented. The GVF allows in principle to reconstruct all "interesting" vertices in a given event, including primary, secondary and two prong particle decay vertices. However, in our particular case, a simplified version of the algorithm is used, tuned to reconstruct just the dimuon secondary vertices. A given reconstructed track was considered to be a muon and was taken into account in the vertex reconstruction, if it had at least two pixel hits and was associated with the true Monte Carlo muon, i.e. no realistic tracker-muon system matching has been implemented yet. We consider that the efficiency for this matching should be very high as the b-jets are relatively soft i.e. open and of moderate multiplicity

while the muons are typically will be of $p_t^\mu \geq 6$ GeV. To understand the vertex quality cuts used below one has to keep in mind that the GVF is a two-step procedure. In this case it creates first the vertex seeds trying all dimuon combinations. A given track pair is accepted as a secondary vertex seed if the minimal 3D distance (called M2D below) between the two spirals is small enough. At this stage some tracks can belong, in principle, to several vertex seeds. At a second stage of the algorithm all accepted seeds are processed by the dedicated algorithm, which tries to solve ambiguities and to fit simultaneously the vertex positions and the track parameters.

Several event samples have been used to optimise the selection criteria and the signal to background ratio.

1. ~ 400 signal events.
2. 3000 signal events with muons only. Other particles in the event were not propagated through the detector. This sample has been used to tune the vertex reconstruction and selection criteria.
3. 10000 background events.
4. 10000 same background events, but bearing only the muons.

The samples with muons only have been used mostly to evaluate the high luminosity scenario, since the processing of a full event (bunch crossing), with pile-up, takes enormous CPU and memory resources at the moment.

The basic variables which characterise the performance of the low luminosity tracker configuration are shown in Figure 2. In this figure one can see dimuon mass resolution, secondary vertex resolution in X/Y and Z coordinates and proper time resolution.

3.2 Selections criteria based on the tracker

i) mass cut

The first background suppression criterion is a $B_s^0 \rightarrow \mu\mu$ mass cut against the continuum dimuon background population. To search for signal events we have chosen a di-muon mass window of ± 40 MeV centred on the B_s mass of 5.369 GeV. In Figure 3a the di-muon mass spectrum for the background is shown after the trigger and initial kinematics selections. The 80 MeV mass window is also shown in the same figure. Only 1.1 ± 0.1 % of background events is retained in this mass window. As full simulations have shown, the high luminosity tracker configuration provides nearly the same di-muon mass resolution. For high luminosity running we thus expect the same selectivity of the dimuon mass cut both for the signal and background as for the low luminosity case.

ii) isolation

$B_s^0 \rightarrow \mu\mu$ decays produced in soft b-jets are semi-isolated and significantly more isolated than dimuons from accidental $g \rightarrow b(\rightarrow \mu)\bar{b}(\rightarrow \mu)$ associations. In our previous study [1] it was found that the rejection factor based on the tracker isolation depends strongly on the lower cutoff on the transverse momentum of the charged particles in the isolation cone around the di-muon momentum. The detailed tracker pattern recognition studies show that charged tracks with transverse momenta above 0.9 GeV can be reconstructed with an efficiency exceeding 90 % within the tracker acceptance [6]. In this work we have used a slightly different tracker isolation definition than in [1]. We required no charged tracks with $p_t > 0.9$ GeV in a cone $\Delta R = 0.5 \times \Delta R_{\mu\mu} + 0.4$ around the di-muon momentum direction. Such a criterion gives an efficiency of 0.49 for the signal and $(3.0 \pm 0.2) \times 10^{-2}$ for the background in conditions of low luminosity running.

Assuming a charged track reconstruction efficiency 0.9 for tracks with $p_t > 0.9$ GeV, we reproduced at the particle-level simulations the efficiency of the tracker isolation criterion obtained with full simulation and pattern recognition: $(2.7 \pm 0.2) \times 10^{-2}$ at the particle level as compared to $(3.0 \pm 0.2) \times 10^{-2}$ with full simulation and pattern recognition. This then allows us to obtain the efficiency of the tracker isolation criterion for the high luminosity case where we didn't make the full detector simulation. Figures 4a,c and Figure 5a,c show the tracker isolation parameter - the number of charged tracks with $p_t > 0.9$ GeV in a cone $\Delta R = 0.5 \times \Delta R_{\mu\mu} + 0.4$ around the di-muon momentum direction obtained with particle-level simulation as explained above for the case of low (Figure 4a,c) and high (Figure 5a,c) luminosity.

iii) secondary vertex selection

A third set of cuts is based on the secondary vertex reconstruction quality and primary-secondary vertex separation. The minimal cuts on the reconstructed secondary vertex applied at the event reconstruction level allows to keep almost all signal events ($\sim 95\%$), but the background rejection factor is then about 4. The di-muon vertex reconstruction algorithm provides however a number of parameters which can be used to improve the vertexing rejection power. After the preliminary analysis, 5 variables were chosen:

1. M2D - minimal distance of approach in space between the two tracks to create the secondary vertex seed (Figure 6).
2. M2D_{rel} - relative minimal distance between the two tracks to create the secondary vertex seed (Figure 7).
3. VTR_{rel} - relative transverse distance (transverse flight path) of the reconstructed secondary vertex to the primary vertex (by relative we mean here the variable measured in terms of its errors). It is shown in Figure 8
4. VTR_{err} - absolute error on the reconstructed secondary vertex in the transverse plane (Figure 9).
5. COS_{pr} - cosine of the angle between the vector pointing to the secondary vertex position (flight path direction) and the two-tracks momentum (B_s^0 momentum) in the transverse plane (Figure 10).

To reject effectively the false background vertices one has to select high quality reconstructed secondary vertices which are rather far away from the primary interaction vertex in the transverse plane. Optimising signal observability, we find that a rejection factor of order 10^{-4} can be obtained. The following set of cuts allows to achieve such a rejection:

1. $VTR_{rel} \geq 12$ (as we checked this cut is nearly equivalent to a sharp cut on the vertex distance in the transverse plane of about 820μ , however, we prefer to use a cut on a variable calculated on an event by event basis)
2. $COS_{pr} \geq 0.9997$
3. $VTR_{err} \leq 80\mu$
4. $M2D \leq 50\mu$
5. $M2D_{rel} \leq 2$

This in fact allows to eliminate ALL events from the 10K background sample for the low luminosity tracker geometry, still keeping about 30 % of the signal. We conclude that the vertexing rejection power is better than 2.3×10^{-4} at the 90% C.L. level.

To obtain the same rejection power for the high luminosity tracker geometry one has to use tighter cuts, in particular changing the cut on the relative transverse distance $VTR_{rel} \geq 12$ to $VTR_{rel} \geq 15$ we can still reject all background events. However, a factor of ≈ 1.8 in signal efficiency is lost. Other combinations of cuts investigated for the high luminosity geometry lead to comparable loss in signal efficiency.

3.3 Selection criterion based on calorimeters

We have also included calorimeter isolation criteria to get an additional background suppression factor. We required no transverse energy in the ECAL plus HCAL above 4 GeV (6 GeV) at $L = 10^{33} cm^{-2} s^{-1}$ ($L = 10^{34} cm^{-2} s^{-1}$) in the same cone as for the tracker isolation. An additional rejection factor of 2.3 ± 0.2 (both for low and high luminosity) to the tracker isolation only has been obtained at the particle-level simulation and checked on the restricted sample of background events with full GEANT simulation. The efficiency of this additional criterion for the signal is 0.94 ± 0.08 for low luminosity and 0.91 ± 0.08 for the high luminosity case. The isolation energy distribution in the calorimeter obtained at particle level is shown in Figure 4b,d for low luminosity running and in Figure 5b,d for the high luminosity case.

3.4 Correlation of the mass and isolation selections

We have checked the correlation between the isolation of the dimuon pair (in the tracker and calorimeter) and the dimuon mass, to check whether it was correct to evaluate independently the efficiency of the mass cut and the isolation criteria.

In Figure 3b the efficiency of the isolation criteria applied to different regions of di-muon mass is shown. One can clearly see a correlation. However, the efficiency of the isolation criterion obtained with full statistics over the whole di-muon mass interval (shown in the Figure 3 b as open marks) coincides within the statistical errors with the one obtained for the proper interval of mass 4-6 GeV where the B_S mass is located. One can also see in Figure 3 b that the calorimeter isolation gives a sufficient additional suppression factor over the entire interval of dimuon mass.

4 Conclusion

Table 1 summarised the efficiency of the selection criteria and the number of signal $B_S^0 \rightarrow \mu\mu$ and background events after successive selection steps, for one year running at both low and high luminosity. Due to insufficient Monte-Carlo statistics we give for the number of background events an upper limit at 90% C.L. As one can obtain from Table 1, the $B_S^0 \rightarrow \mu\mu$ decay should be seen with significance 4 after 3 year of running at a luminosity of $L = 10^{33} \text{cm}^{-2} \text{s}^{-1}$ even if the background were underestimated by a factor 2. With $3 \times 10^4 \text{pb}^{-1}$ data at low luminosity ($10^{33} \text{cm}^{-2} \text{s}^{-1}$) and 10^5pb^{-1} at high luminosity ($10^{34} \text{cm}^{-2} \text{s}^{-1}$) significance 6.3 can be achieved. This more optimistic expectation when compared to our previous study [1] comes from the more sophisticated algorithms for the track and vertex reconstruction and the tighter vertex selection criteria.

Taking into account the $B^0/B_S^0 = 0.40/0.11$ production ratio and the expected Standard Model $Br(B_d^0 \rightarrow \mu\mu) = (1.5 \pm 0.9) \times 10^{-10}$, we also estimated that we should get for one year running at low luminosity (1.1 ± 0.7) of $B_d^0 \rightarrow \mu\mu$ decays again on essentially no background.

We should mention again that in the evaluation of the number of the signal and background events we have assumed 100 % efficiency of the High Level Triggers for this di-muon channel. This might not be exactly the case although only a minor loss is expected, but a special study of the High Level Triggers efficiency for this mode is now under way. Also we assumed full efficiency for tracker-muon chamber muon track matching; preliminary studies [8] indicate that it is ≥ 90 %.

Table 1. Selection efficiencies and number of signal and background events before and after selections for 10^4pb^{-1} running at low ($L = 10^{33} \text{cm}^{-2} \text{s}^{-1}$) and 10^5pb^{-1} running at high ($L = 10^{34} \text{cm}^{-2} \text{s}^{-1}$) luminosity.

| | Signal | Background |
|--|--------|---------------------------|
| number of events after trigger and kinematics selections | 66 | 2.9×10^7 |
| tracker isolation. Low luminosity | 0.49 | 3.0×10^{-2} |
| tracker isolation. High luminosity | 0.34 | 2.0×10^{-2} |
| tracker+calo isolation. Low luminosity | 0.46 | 1.3×10^{-2} |
| tracker+calo isolation. High luminosity | 0.31 | 0.87×10^{-2} |
| 2 - μ rec. + sec.vertex selections. Low luminosity | 0.32 | $\leq 2.3 \times 10^{-4}$ |
| 2 - μ rec. + sec.vertex selections. High luminosity | 0.18 | $\leq 2.3 \times 10^{-4}$ |
| mass window 80 MeV | 0.72 | 1.1×10^{-2} |
| number of events after cuts. Low luminosity | 7.0 | ≤ 1.0 at 90% C.L. |
| number of events after cuts. High luminosity | 26.0 | ≤ 6.4 at 90% C.L. |

5 Acknowledgements

We are thankful to D. Denegri, Y. Lemoigne and all members of the CMS B-physics group for discussions and comments. We specially thank to D. Denegri for careful reading of this note and very useful

corrections.

References

- [1] A. Nikitenko, A. Starodumov, CMS TN/94-186.
- [2] A. Ali, “Flavour Changing Neutral Current Processes in B Decays”, DESY 97-019, February 1997
- [3] T.Sjostrand. *Comp.Phys.Comm.* 82 (1994) 74; CERN-TH.6488/92; CERN-TH.7112/93 (revised February 1994)
- [4] C.Peterson et al. *Phys.Rev.D*27 (1983) 105.
- [5] **CMSIM User’s Guide at WWW. <http://cmsdoc.cern.ch/swsi.html>.**
- [6] The Tracker Project Technical Design Report. CERN-LHCC-98-6, CMS TDR5 (1998)
- [7] N.Stepanov, A.Khanov, *Nucl.Inst.Meth.* A389 (1997) p.177
- [8] private communications

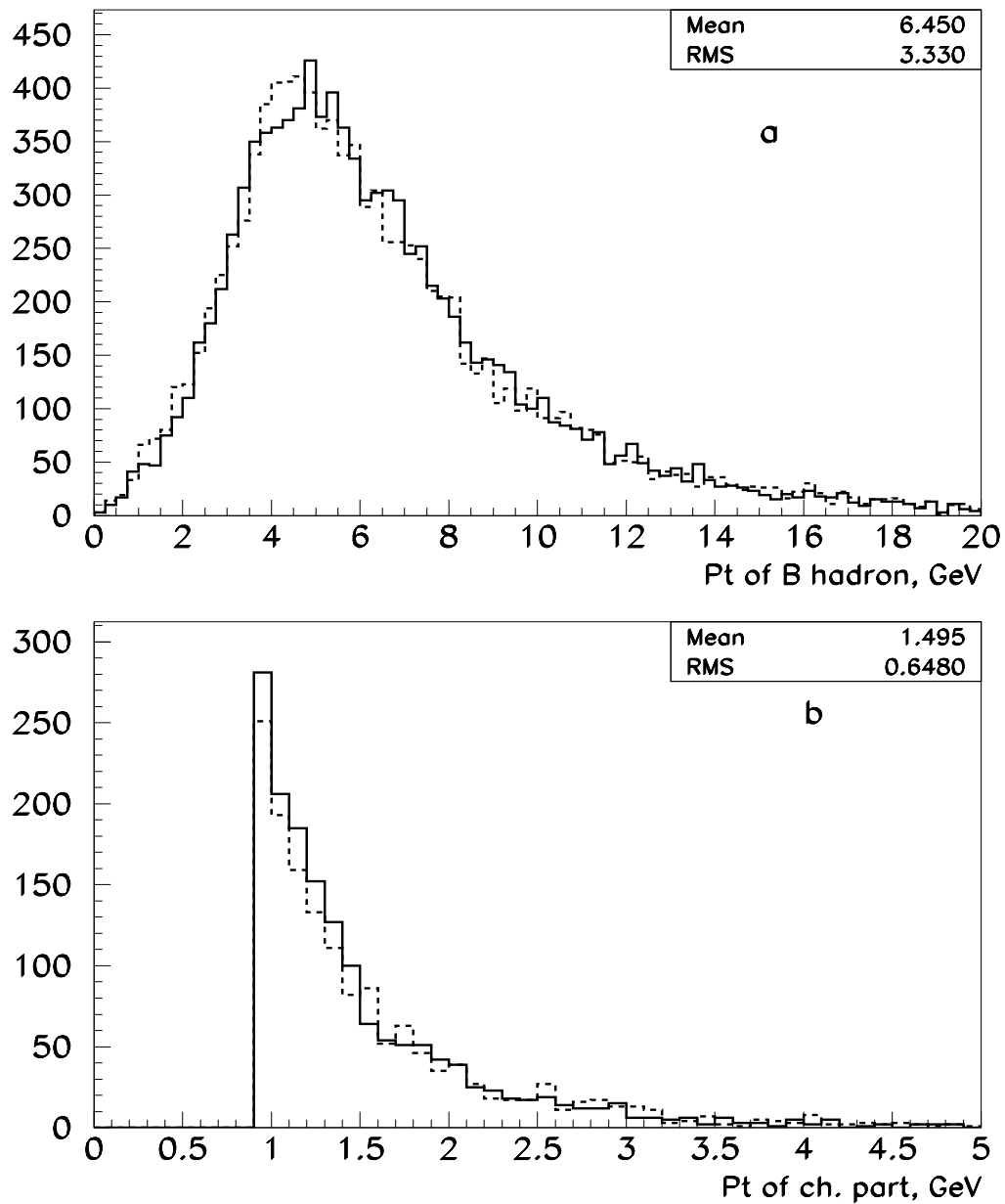


Figure 1: p_t spectra of B hadron (a) and charged particles (b) (not including decay products of B-hadron) in cone 0.4 around B-hadron for different choice of fragmentation function in PYTHIA5.7. Solid line - PYTHIA5.7 default MSTJ(11)=4, dashed line - Peterson fragmentation MSTJ(11)=3

resolutions for $|\eta_\mu| < 2.4$ (acceptance = 100%)

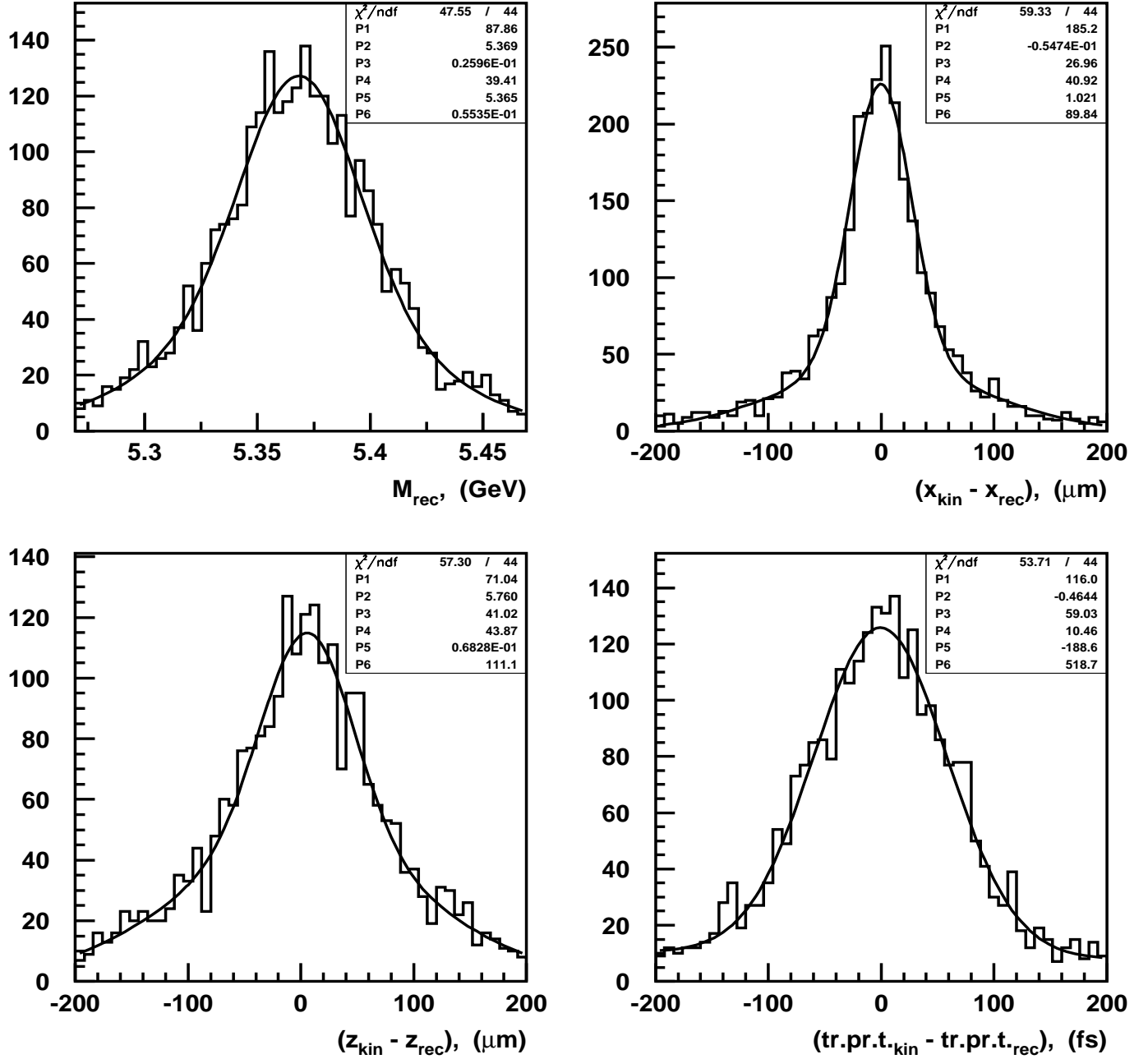


Figure 2: Signal events. Dimuon mass resolution, resolution in X/Y, resolution in Z, time resolution

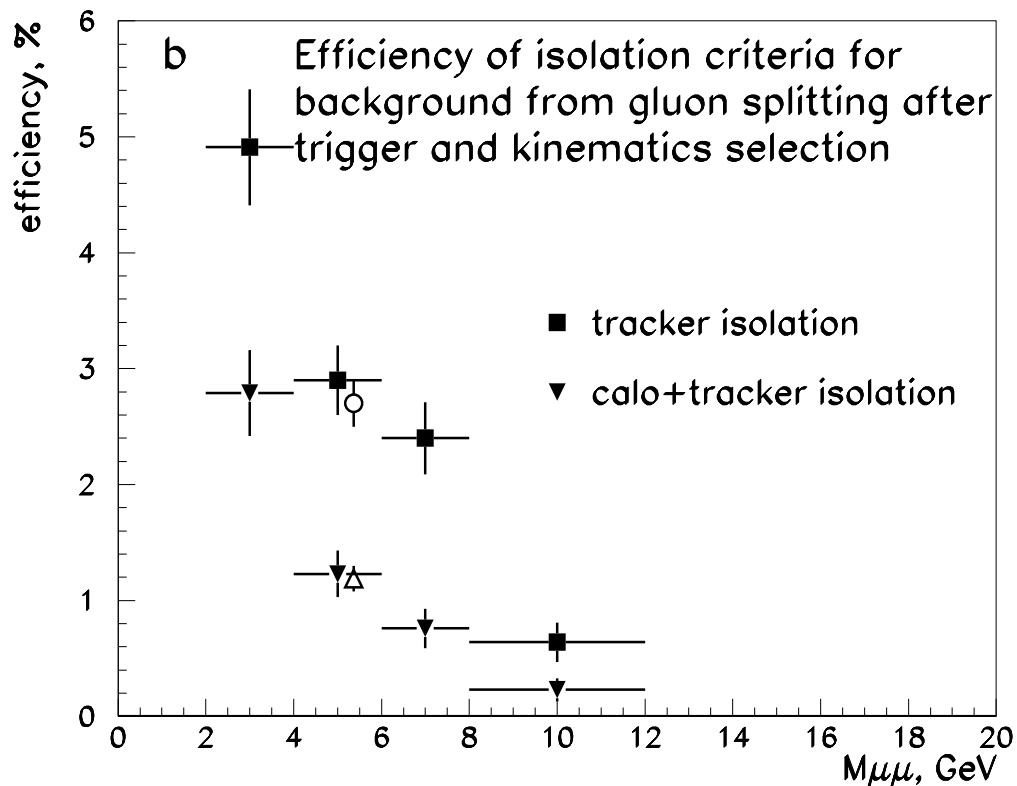
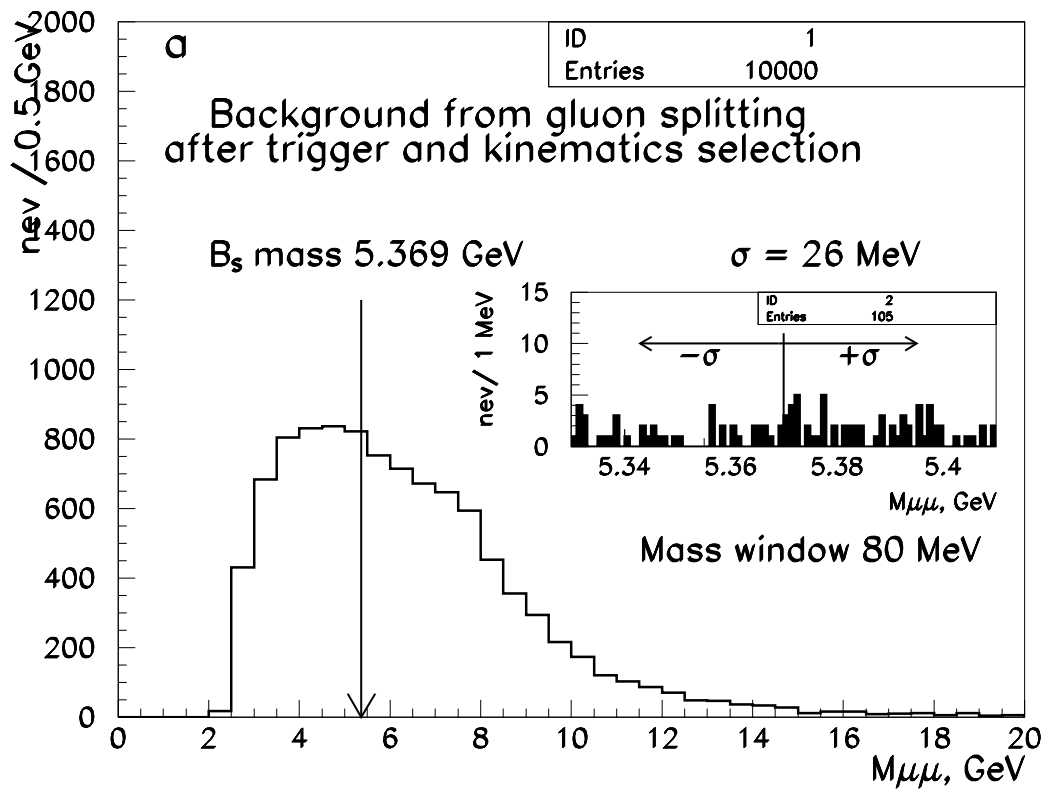


Figure 3: a) - dimuon mass spectrum for the background from gluon splitting after the trigger and kinematics selection. A mass window 80 MeV for the signal search is shown together with the signal resolution in the insertion. b) - efficiency of the isolation criterion with the tracker only and with the tracker and calorimeter combined for the background from gluon splitting, after the trigger and kinematics

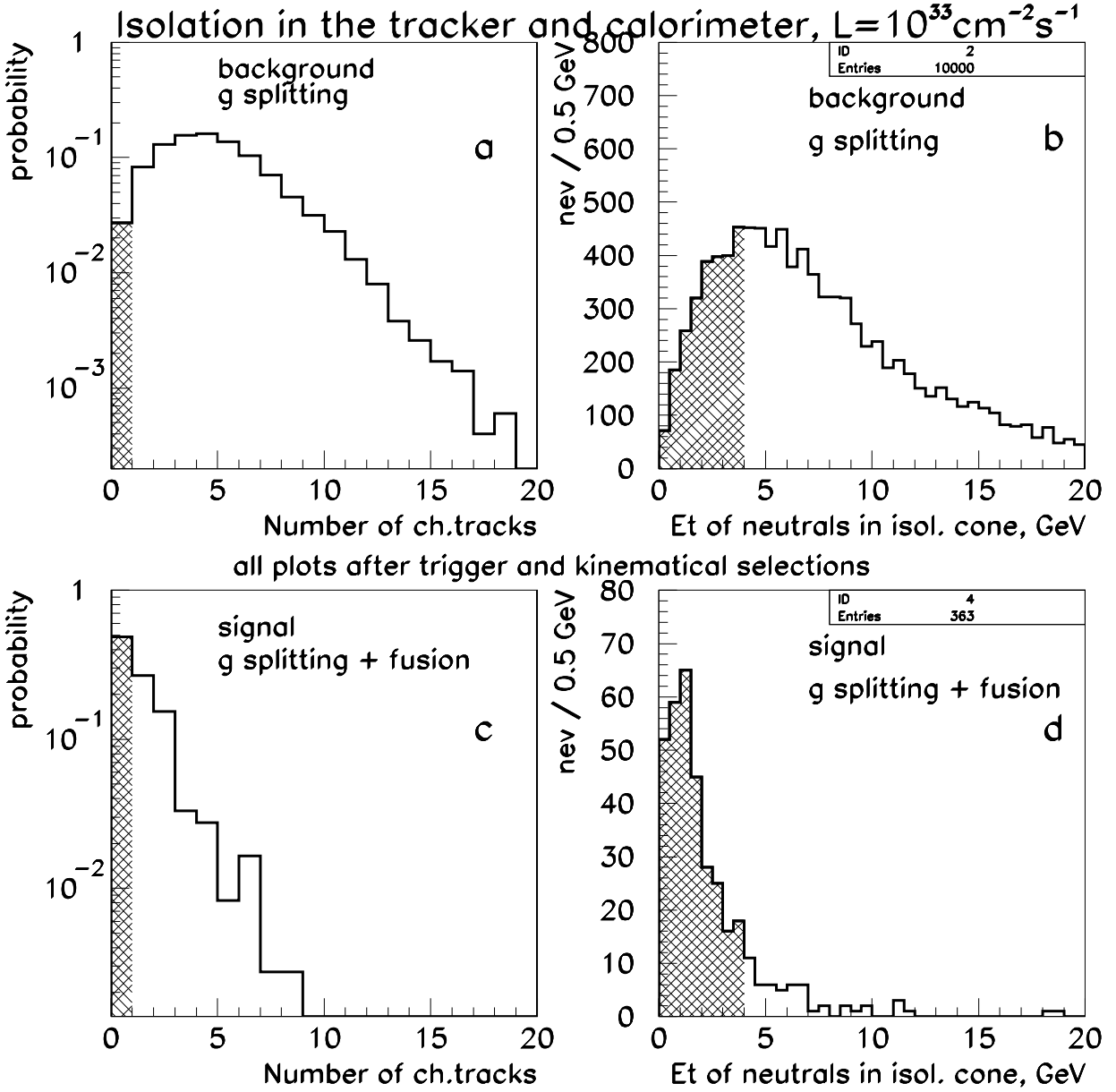


Figure 4: Tracker isolation parameter (see text) for the background (a) and signal (b), calorimeter isolation energy for the background (b) and signal (d) calculated with particle level simulation (as explained in the text) for the case of $L = 10^{33} \text{ cm}^{-2} \text{ s}^{-1}$.

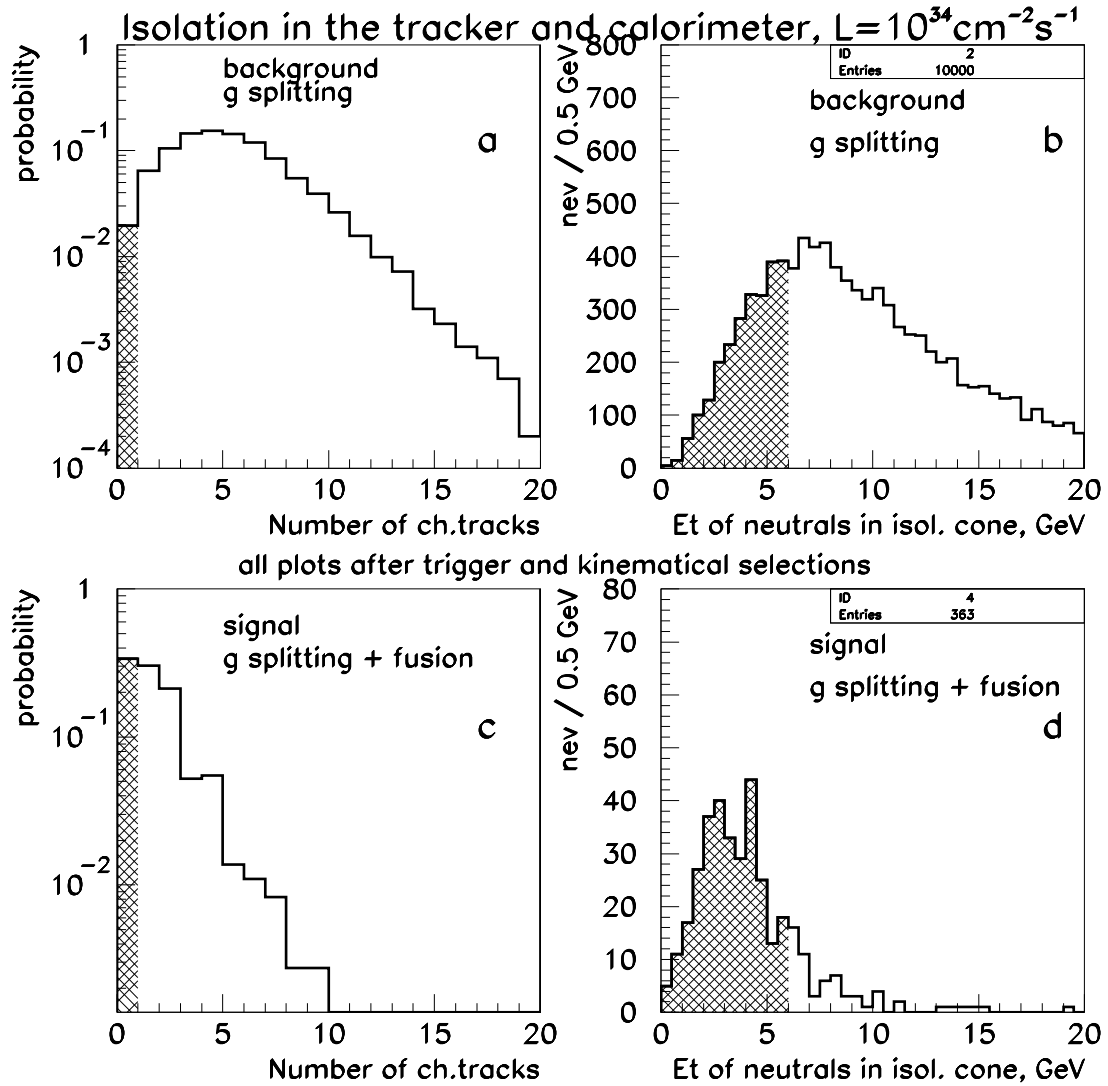


Figure 5: Tracker isolation parameter (see text) for the background (a) and signal (b), calorimeter isolation energy for the background (b) and signal (d) calculated with particle level simulation (as explained in the text) for the case of $L = 10^{34} \text{cm}^{-2} \text{s}^{-1}$.

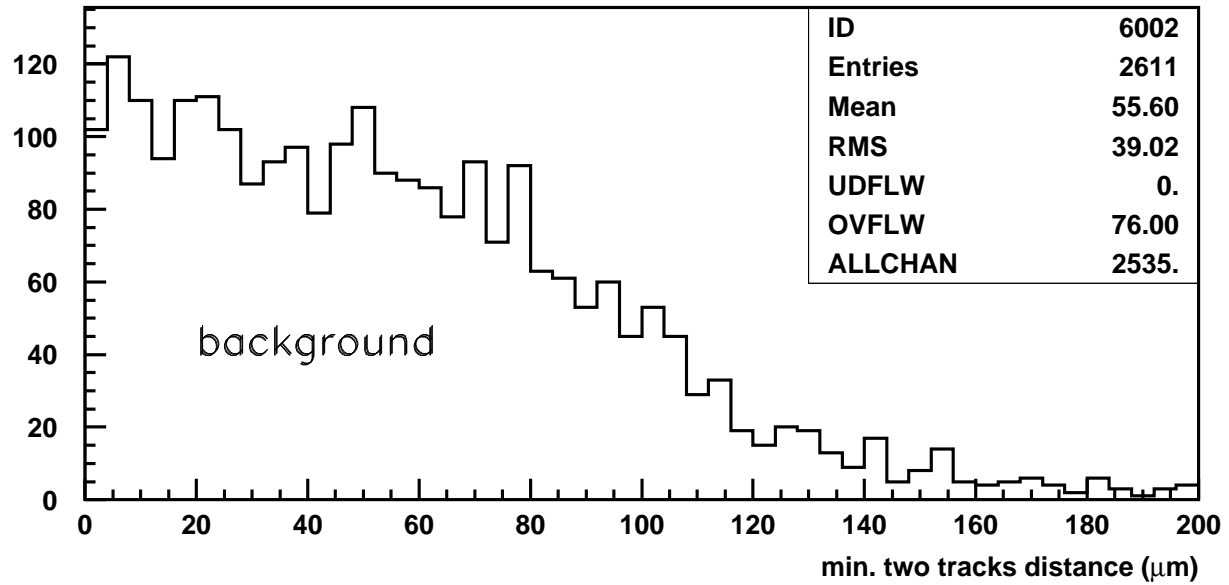
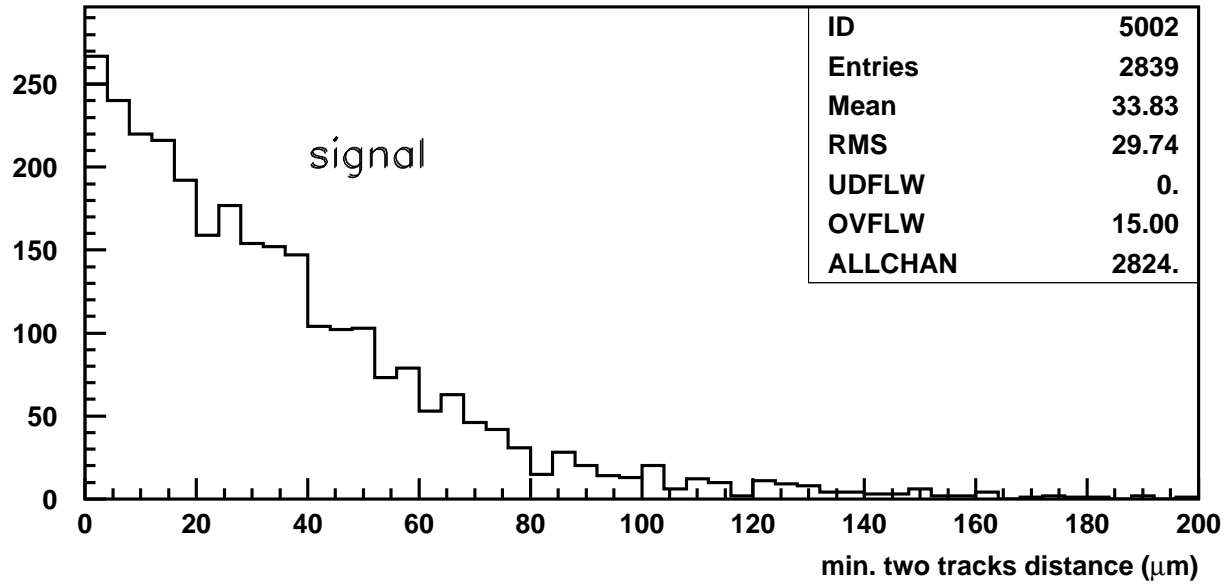


Figure 6: Minimal distance in space between two muon tracks for the signal and background

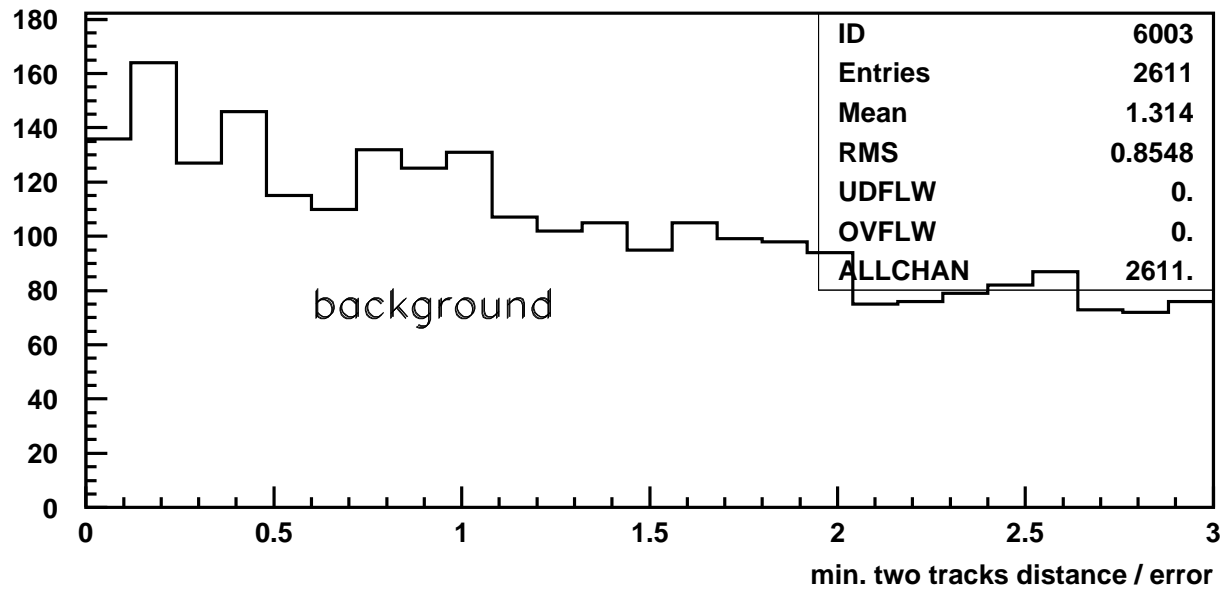
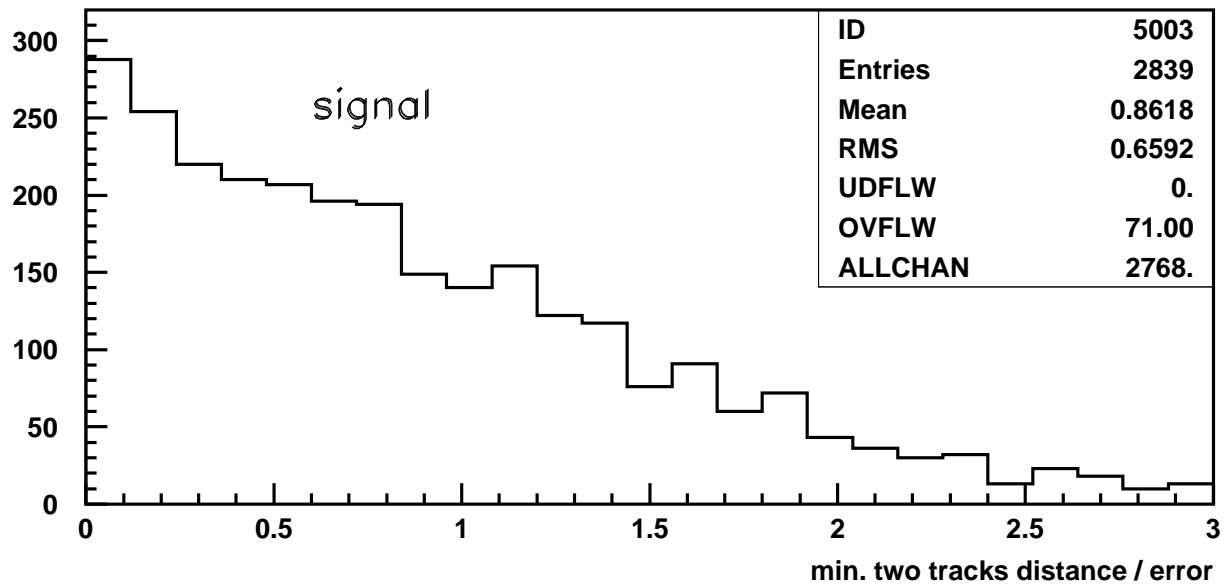


Figure 7: Minimal distance in space between two muon tracks divided by the error of this value for the signal and background

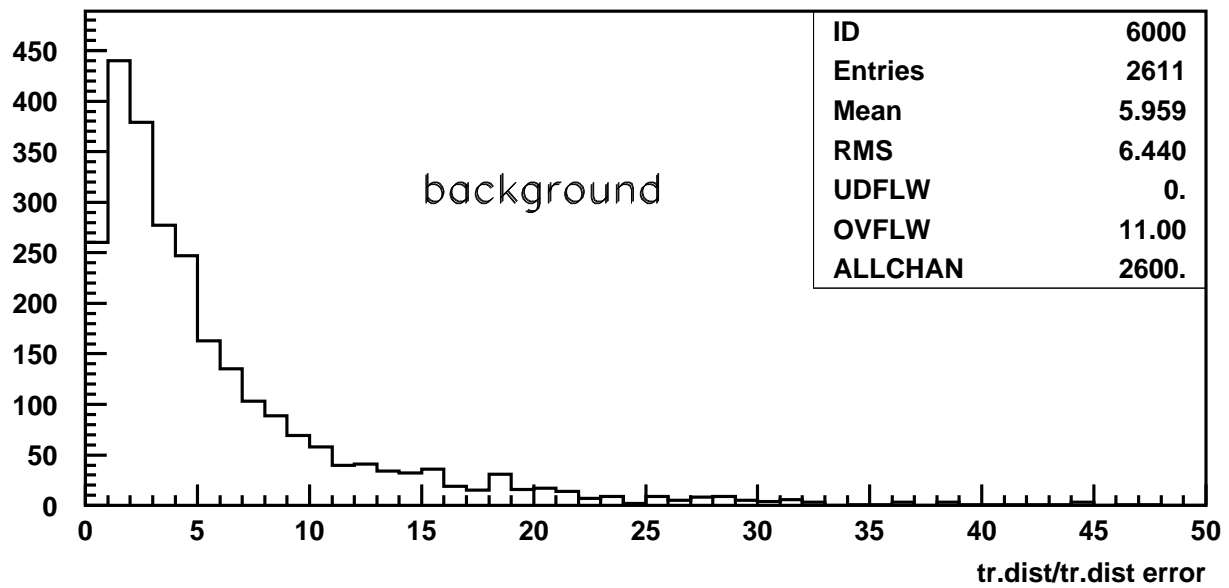
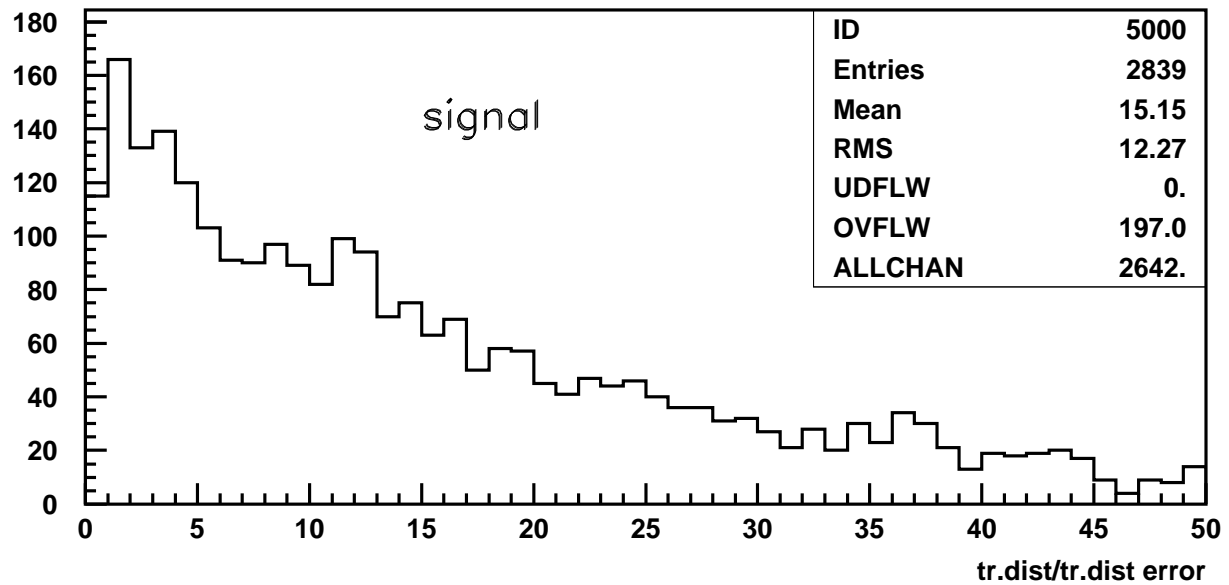


Figure 8: Transverse distance (flight path) between secondary and primary vertex divided by the error of this quantity for signal and background

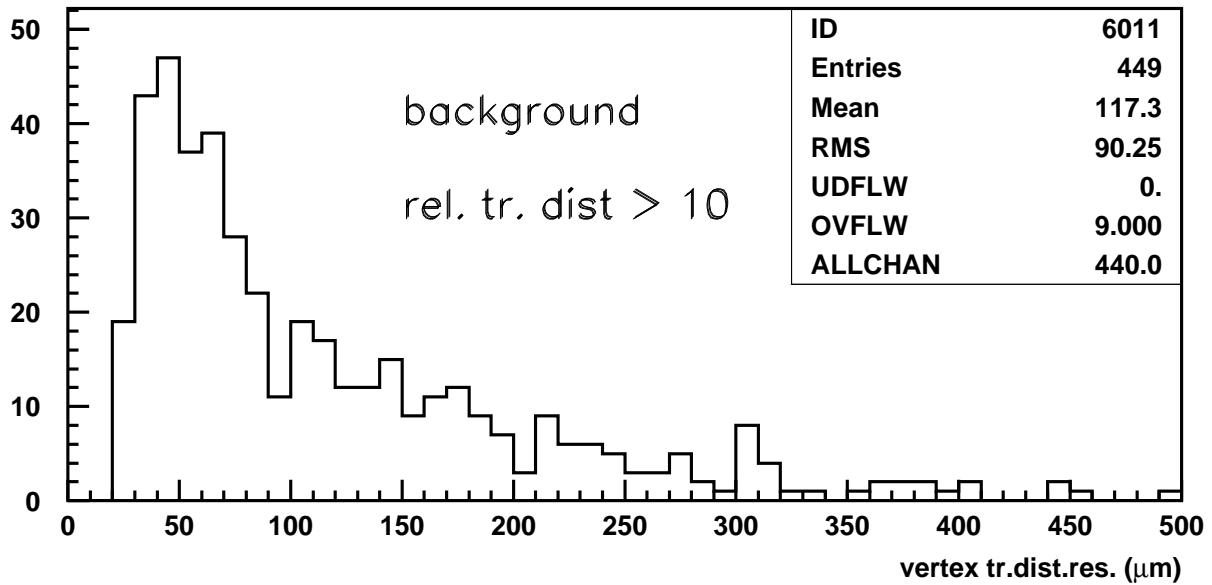
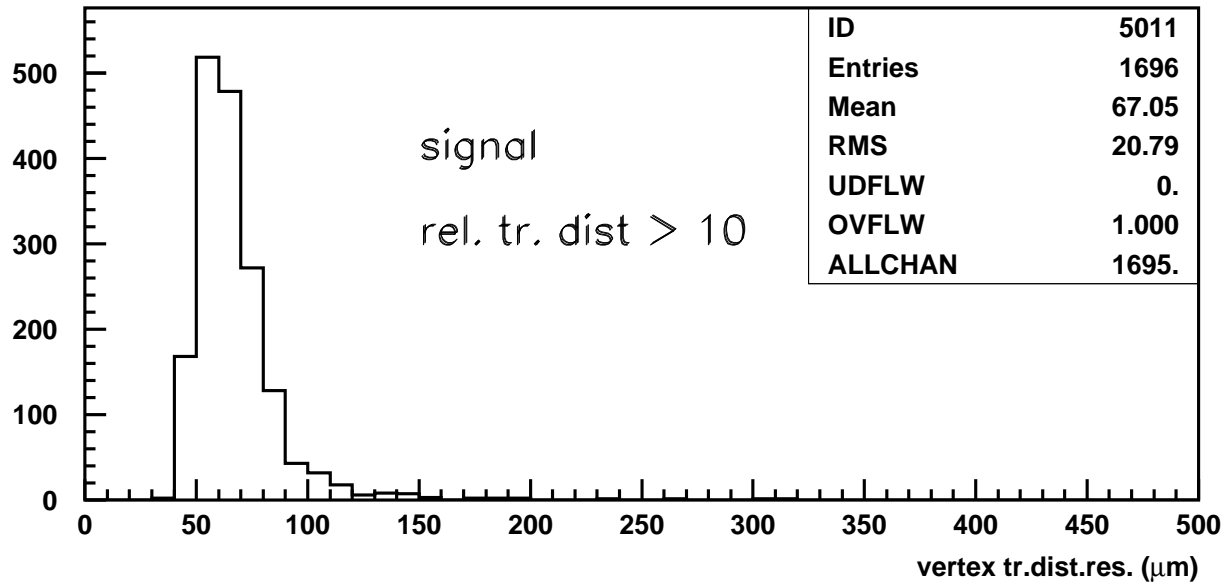


Figure 9: Error on the transverse distance (flight path) between primary and secondary vertices for the signal and background

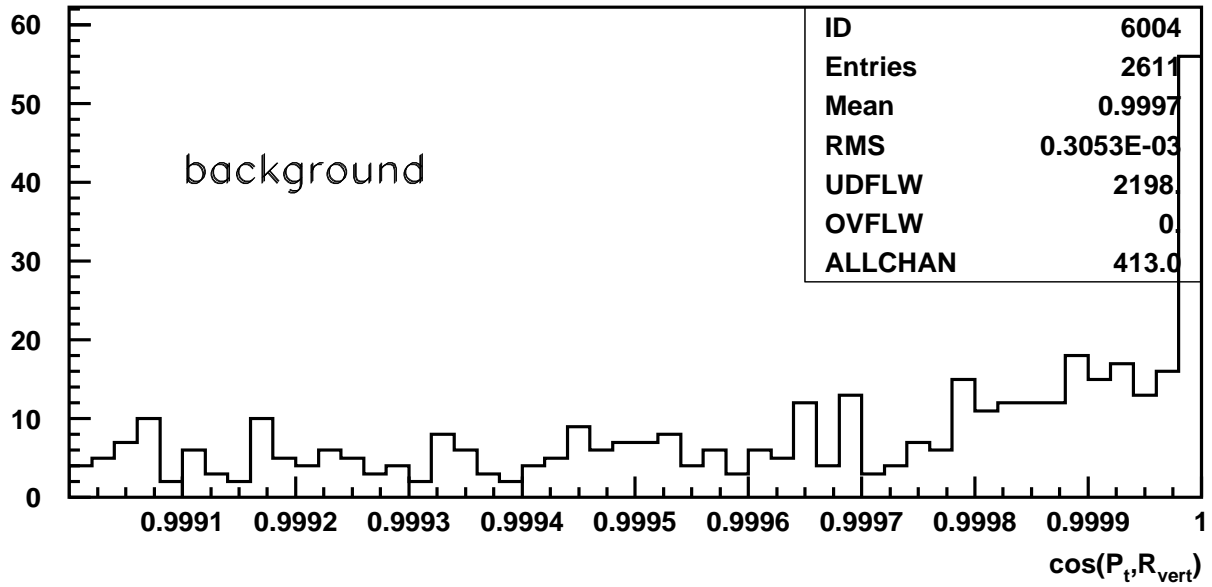
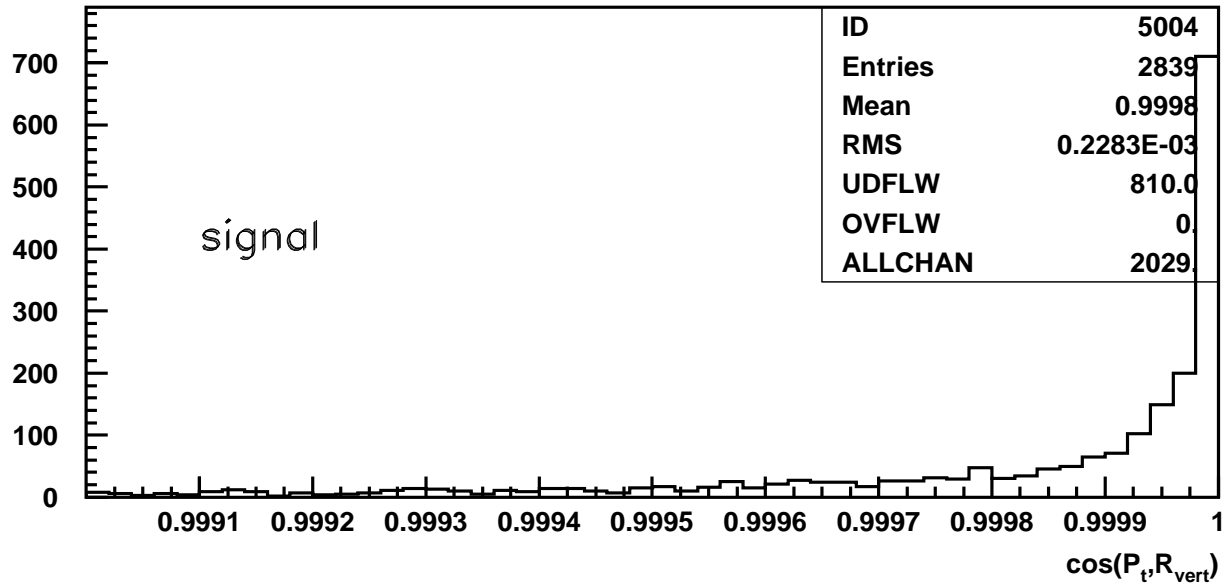


Figure 10: Cosine of the angle in the transverse plane between the vector pointing from the primary to secondary vertex (flight path) and the dimuon transverse momentum